Article

Aluminium-Based Dissimilar Alloys Surface Composites Reinforced with Functional Microparticles Produced by Upward Friction Stir Processing

Filipe Moreira [1], Pedro M. Ferreira [1], Rui J. C. Silva [2], Telmo G. Santos [1,3] and Catarina Vidal [1,3,*]

[1] UNIDEMI, Department of Mechanical and Industrial Engineering, NOVA School of Science and Technology, Universidade NOVA de Lisboa, 2829-516 Caparica, Portugal; faf.moreira@campus.fct.unl.pt (F.M.); pdm.ferreira@campus.fct.unl.pt (P.M.F.); telmo.santos@fct.unl.pt (T.G.S.)

[2] CENIMAT/i3N, Departamento de Ciência dos Materiais, NOVA School of Science and Technology, Universidade NOVA de Lisboa, 2829-516 Caparica, Portugal; rjcs@fct.unl.pt

[3] Laboratório Associado de Sistemas Inteligentes, LASI, 4800-058 Guimarães, Portugal

* Correspondence: c.vidal@fct.unl.pt

Abstract: Surface metal matrix composites offer an excellent solution for applications where surface properties play a crucial role in components' performance and durability, such as greater corrosion resistance, better wear resistance, and high formability. Solid-state processing techniques, such as friction surfacing and friction stir welding/processing, offer several advantages over conventional liquid-phase processing methods. This research investigated the feasibility of producing surface composites of aluminium-based dissimilar alloys reinforced with functional microparticles through experimental validation, determined the process parameters that resulted in a more homogeneous distribution of the particles in the surface composites, and enhanced the understanding of Upward Friction Stir Processing (UFSP) technology. The production of aluminium-based dissimilar alloys (AA 7075-T651 and AA 6082-T651) surface composites reinforced with SiC particles was studied, and it was concluded that the macrography and micrography analyses, scanning electron microscopy (SEM) analysis, microhardness measurements, and eddy currents technique reveal an extensive and homogeneous incorporation of SiC particles. In the stirred zone, a decrease of approximately 20 HV 0.5 in hardness was observed compared to the base material. This reduction is attributed to the weakening effect caused by low-temperature annealing during UFSP, which reduces the strengthening effect of the T651 heat treatment. Additionally, the presence of particles did not affect the surface composite hardness in the stirred zone. Furthermore, despite the presence of significant internal defects, SEM analyses revealed evidence of the lower alloy merging with the upper zone, indicating that the lower plate had a role beyond being merely sacrificial. Therefore, the production of bimetallic composites through UFSP may offer advantages over composites produced from a monometallic matrix. The results of the eddy currents testing and microhardness measurements support this finding and are consistent with the SEM/EDS analyses.

Keywords: upward friction stir processing; surface composites; metal matrix composites; aluminium alloys; SiC particles; surface modification

1. Introduction

Metal matrix composites (MMCs) have emerged as promising materials for various structural applications owing to their ability to improve the specific strength of pure metals or alloys by incorporating secondary phase particles. Materials such as aluminium, copper, magnesium, and titanium are commonly used as matrix materials, while particles such as SiC, SiO_2, Al_2O_3, TiB_2, $BaTiO_3$, graphene, and WC are often used as secondary phase materials [1–8]. MMCs find applications in industries such as automobile, aerospace, marine, and power generation due to their enhanced fatigue and wear resistance. Stir

casting, squeeze casting, spray deposition, in situ fabrication, powder metallurgy, and friction stir processing (FSP) are a few examples of manufacturing technologies commonly used to fabricate MMCs [9–12].

There are certain applications where surface properties play a crucial role in components' performance and durability. Surface MMCs, which contain dispersed secondary phase particles only at the surface while the core remains unaffected, offer an excellent solution for such cases. The surface of these composites exhibits higher hardness and wear resistance, while the bulk material retains its toughness [13]. Various methods, such as laser-assisted processes, centrifugal casting, and plasma spraying, have been developed to fabricate surface MMCs [13–17] and involve the transformation of material from a solid to liquid or vapor state during processing.

In contrast, solid-state processing techniques that do not involve material transformation to the liquid phase during processing offer several advantages over conventional liquid-phase processing methods. Friction surfacing and friction stir welding/processing (FSW/P) are prominent examples of solid-state processing technologies that are used to modify surfaces and develop surface composites [18–23].

FSW/P has shown great potential in processing dissimilar materials with different properties, such as high strength and high corrosion resistance. Joining dissimilar materials can be challenging due to their different properties, but FSW/P has been successfully used by researchers to join dissimilar materials and investigate their corrosion resistance and metallographic and mechanical properties [24–27]. FSW is also suitable for welding low melting point materials and has been used to join low–high melting point metals, such as an aluminium alloy to steel, making it a popular area of research.

Proper material mixing is crucial in FSW/P as it plays a significant role in joint formation. Previous studies have investigated the properties of FSW/P joints of various aluminium alloys, including AA 2219 and AA 7475 [28], AA 5083 and AA 6082 [29,30], AA 2024 and AA 6056 [31], and AA 2024 and AA 6061 [32]. These studies focused on the mechanisms of material mixing and microstructure development in the stirred zone, which greatly affects the joint's strength.

Several studies have been conducted to investigate the influence of material location with respect to tool rotation on joint properties in FSW/P. The findings suggest that material position, rotational speed, and traverse speed significantly impact plastic flow behaviour, grain structure, and joint quality [33–35]. Research conducted by Guo et al. [36] on AA 6061-AA 7075 showed that effective material mixing and the highest joint strength was achieved at the highest traverse speed when AA 6061 was positioned on the advancing side (AS) and AA 7075 on the retreating side (RS). Sahu et al. [37] studied the impact of material location on the mechanical properties of FSW joints fabricated from aluminium/copper and found that a higher joint strength was attained by positioning the copper on the AS. Other studies, such as those carried out by Cavaliere et al. [38] and Dinaharan et al. [39], also showed that the superior joint was produced by locating the higher strength aluminium alloy on the AS. However, few studies have reported effective material mixing by locating lower grades on AS.

Previous research has extensively studied FSW/P of dissimilar aluminium alloys. However, dissimilar FSW of 6xxx and 7xxx series aluminium alloys has received limited attention. These two series of aluminium alloys are widely used as structural parts in transportation and aircraft industries and are heat treatable. The location of the materials influences the material mixing and flow behaviour, which are crucial mechanisms for joint formation [37,40,41]. Although several studies have investigated the FSW/P of dissimilar aluminium alloys, to the best of the authors' knowledge, no work has been reported on producing aluminium-based dissimilar alloys surface composites reinforced with functional microparticles using AA6082 and AA7075 as base materials. Therefore, the main objectives of this study were to investigate the feasibility of producing surface composites of aluminium-based dissimilar alloys reinforced with functional microparticles through experimental validation, determine the process parameters that result in a more homoge-

neous distribution of particles in the composites' surface, and enhance the understanding of Upward Friction Stir Processing (UFSP) technology. Existing FSP-based techniques do not ensure a three-dimensional distribution of functional particles, resulting in a non-uniform distribution and significant cluster formation [3]. Tool wear is also a significant issue when using hard abrasive particles to reinforce aluminium-based matrices. So, a new FSP-based technique developed by Inácio et al. [42] called UFSP was proposed, which promotes an upward viscoplastic material flow to pull up functional particles from the bottom of the tool probe to its top, resulting in a more uniform and three-dimensional distribution of particles in the metal matrix. Various characterization techniques were employed in this study, including macrography and micrography analyses, scanning electron microscopy (SEM) and X-ray energy-dispersive spectrometer (EDS) analyses, and microhardness and eddy currents measurements.

2. Materials and Methods

2.1. Materials

Two different metallic materials were used in the experimental tests: aluminium alloy 6082-T651 and aluminium alloy 7075-T651, which have a wide range of industrial applications. Aluminium alloys 6082 and 7075 are commonly used in structural components for various industries, including naval, aeronautics, automotive, and military, among others.

Commercial plates with dimensions of 203 (rolling direction) × 103 mm and a thickness of 3 mm were used in this work. Table 1 shows the chemical composition of AA 7075-T651 and AA 6082-T651.

Table 1. Chemical composition of AA 7075-T651 and AA 6082-T651, wt%.

Elements	AA 7075-T651	AA 6082-T651
Al	87.1–91.4	95.4–98.3
Mg	2.1–2.9	0.6–1.2
Zn	5.1–6.1	≤0.2
Cu	1.2–2.0	≤0.1
Si	≤0.4	0.7–1.3
Mn	≤0.3	0.4–1
Fe	≤0.5	≤0.5
Ti	≤0.2	≤0.1
Cr	-	≤0.25

As part of the characterization of AA6082-T651, Vickers hardness measurements were taken in three different planes using a Mitutoyo HM-112 microhardness testing machine. The purpose of this was to verify if there were any variations in hardness across the planes and to determine their average value. Five indentations were made in each plane, with a load of 0.5 kgf and a 1 mm spacing between indentation. The results showed that variations in microhardness values across the three planes were not significant and that AA6082-T651 had an average hardness of 118 HV0.5. The characterization of the other metallic alloy (AA 7075-T651) was carried out by the authors in previous works [42,43]. Table 2 shows the mechanical, electrical, and thermal properties of the two base materials used in this work.

During the experimental tests, reinforcement particles were incorporated onto the surface of the metallic alloys to produce a surface composite. Silicon carbide (SiC) particles, a high-hardness ceramic material, were used as reinforcement as they can increase the hardness of the metallic matrix. Metal matrix composites with SiC particles incorporated in an aluminium matrix can be of interest in industries, such as aerospace, automotive, military, and sports [44]. For the study of dissimilar composites' production, SiC particles with a purity of 99.5% were used, although many other functional particles can be used depending on the desired functionality for the base material. The SiC particles had non-uniform shapes and sizes ranging between 4 and 20 μm, with an average diameter of

6 µm [45]. Figure 1 shows the morphology and dimensions of the SiC particles observed through scanning electron microscopy (SEM) [42].

Table 2. Mechanical, electrical, and thermal properties of AA 7075-T651 and AA 6082-T651.

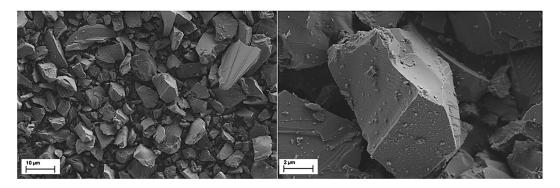| Properties	AA 7075-T651	AA 6082-T651
Density [g/cm^3]	2.83	2.70
Melting point [°C]	475	555
Electrical conductivity [W m^{-1} K^{-1}]	153	170
Modulus of elasticity [GPa]	72.0	70.0
Vickers hardness [HV0.5]	180	118
Ultimate tensile strength [MPa]	550	290
Yield tensile strength [MPa]	490	250
Elongation at fracture [%]	8	10

Figure 1. Scanning electron microscopy images of SiC particles' morphology and dimensions (adapted from [42]).

2.2. Methods

Surface composites were developed by embedding SiC particles within metallic plates using the UFSP variant. This variant differs from existing methods by inducing an "aspiration" effect that promotes the upward flow of reinforcement particles rather than bringing them from an upper level to a lower one. The process involves using two plates with the functional particles placed between them and promoting the upward flow effect by rotating the tool in a counterclockwise direction while using a left-hand threaded tool pin. To ensure uniform distribution of the particles, a spacer made of Kapton® tape was used, which also prevented particle sputtering. The particles were placed between two plates and surrounded by Kapton® tape to prevent wastage and enable the compacting of the particles during thermomechanical processing. The experimental setup, depicted in Figure 2, was mounted on a backing plate and secured by four M8 bolts, and rotational and traverse speeds are represented by ω and v, respectively.
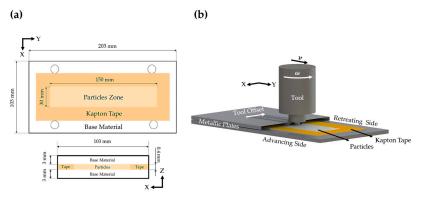

Figure 2. Experimental setup of surface composites production by UFSP: (**a**) top view and transversal view; (**b**) 3D schematic.

To produce a surface composite via UFSP, a tool made of H13 steel was employed. A pin model was utilized: a triflute left-hand threaded 14° conical pin with a bottom diameter of 5 mm was used (Figure 3). The pin had left-hand threads, and since the tool operated with a counterclockwise rotation during the tests, it enabled an upward flow of the base material. Figure 3 illustrates the pin utilized as well as the concave shoulder with a 19 mm diameter.

Figure 3. UFSP tool: concave shoulder with triflute left-hand threaded conical pin.

In recent years, studies have been conducted on UFSP to understand the influence of process parameters on particles' distribution. The effects of shoulder and pin geometry, rotational and traverse speeds, particles volume, and offset between passes were investigated [42,43].

In this study, slower traverse speeds and higher rotational speeds were used compared to previous UFSP studies. This decision was based on the scientific literature on FSW regarding overlapped dissimilar aluminium joints where the best results were obtained within a range of 1000–2000 rev/min and 20–120 mm/min [46–48]. Therefore, experimental tests were performed with a wider range of speeds than in previous UFSP studies [42,43]. In all tests, the tool offset (Figure 2b) was 0.5 mm between passes, and the tool tilt angle was 1°. When using a triflute left-hand threaded conical pin, its length was 4.8 mm in tests without particles and 5.5 mm in tests with particles. Tables 3 and 4 describe all experimental tests performed in this study and the corresponding process parameters.

Table 3. Experimental tests performed and the corresponding process parameters using the experimental setup with an upper AA 7075-T651 plate and a lower AA 6082-T65 plate.

Schematic	Samples without Particles AA7_6_	Samples with Particles AA7_6_	ω	v	No. Processing Passes	Tool Geometry
	1400/45	1400/45_P		45		
	1400/71	1400/71_P	1400	71		
	1400/180	1400/180_P		180		Triflute left-hand threaded conical pin with a 4.8/5.5 mm length
	1120/45	1120/45_P		45	3	
	1120/71	1120/71_P	1120	71		
	1120/180	1120/180_P		180		
	900/180	900/180_P	900	180		

After UFSP, the samples underwent several characterization techniques. Macrography and micrography samples were sectioned (Figure 4) and polished following standard metallographic procedures and then etched using Keller reagent (2 mL HF, 3 mL HCl, 20 mL HNO$_3$, and 175 mL H$_2$O) for 15 s.

Table 4. Experimental tests performed and the corresponding process parameters using the experimental setup with an upper AA 6082-T65 plate and a lower AA 7075-T651 plate.
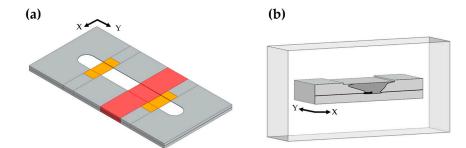
Schematic	Samples without Particles AA6_7_	Samples with Particles AA6_7_	ω	v	No. Processing Passes	Tool Geometry
	1400/45	1400/45_P		45		
	1400/71	1400/71_P	1400	71		
	1400/180	1400/180_P		180		Triflute left-hand threaded conical pin with a 4.8/5.5 mm length
	1120/45	1120/45_P		45	3	
	1120/71	1120/71_P	1120	71		
	1120/180	1120/180_P		180		
	900/180	900/180_P	900	180		

(a)

(b)

Figure 4. Schematic of samples prepared for characterization techniques: (**a**) analyzed sections; (**b**) section embedded in resin for macroscopic and microscopic characterization.

Macrography and micrography analyses were carried out using a Leica DMI 5000 M (Leica Camera, Wetzlar, Germany) inverted optical microscope to reveal the microstructure and particle distributions. High-resolution images of the cross-sections were obtained by combining sequential images.

To obtain a more detailed characterization of the samples, scanning electron microscopy (SEM) was performed using ZEISS DSM 962 equipment (Carl Zeiss AG, Oberkochen, Germany), and the corresponding X-ray energy-dispersive spectrometer (EDS) with an INCA x-act detector (SDD = 10 mm^2) from Oxford Instruments (Abingdon, UK) was used to assess the elemental chemical composition. SEM images were recorded using secondary electrons. A thin conductive gold coating was applied on the SiC particles to improve the conductivity.

The Vickers microhardness profile along the X direction of the processed plate was measured using a Mitutoyo HM-112 hardness testing machine (Mitutoyo Corporation, Sakado, Japan, according to the standard ASTM E384-10. The top surface of the sample was machined, ground, and polished to obtain a homogeneous surface condition. The spacing between consecutive indentations was 1 mm. A load of 0.5 kgf was applied for 10 s.

Eddy currents were used to characterize the microstructural variations and particle distributions across the composites' surface. Variation in the electrical conductivity was measured along a straight line along the X direction, and to obtain a homogeneous surface of the samples, 1 mm of the top surface was machined down (Figure 4a). The eddy currents technique was implemented using a pencil probe operating at 1 MHz and a NORTEC 600D impedance analyzer (Olympus Corporation, Tokyo, Japan). The procedure was developed according to Ferreira et al. [1].

3. Results and Discussion

3.1. Aluminium-Based Dissimilar Alloys Surface Composites

Initially, experimental tests were conducted without particles using an upper AA 7075-T651 plate and a lower AA 6082-T651 plate with the aim of defining the process parameters in order to produce a surface composite. In these tests, it was observed that

the best results were obtained with lower traverse speeds and higher rotational speeds, which is in accordance with the literature on the FSW of dissimilar overlapped joints [46,47]. Figure 5 shows macrographs of samples produced in the tests, including AA7_6_1400/71, AA7_6_1120/180, and AA7_6_900/180, which exhibited smaller internal defects and were stable within the process parameters window presented in Tables 3 and 4.
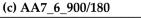

(a) AA7_6_1400/71

(b) AA7_6_1120/180

(c) AA7_6_900/180

Figure 5. Macrography of aluminium-based dissimilar alloys composites produced by UFSP with a lower plate of AA 6082-T651 and an upper plate of AA 7075-T651: (**a**) AA7_6_1400/71; (**b**) AA7_6_1120/180; (**c**) AA7_6_900/180.

Figure 6 shows macrographs of the samples produced in the AA7_6_1400/71, AA7_6_1120/180, and AA7_6_900/180 tests, which were conducted without particles and with the lower plate made of AA 6082-T651 and the upper plate made of AA 7075-T651. In Figure 6, the magnified regions highlight the microstructure of the unaffected zone (base material), the heat affected zone (HAZ), the thermo-mechanically affected zone (TMAZ), and the dynamic recrystallization zone (nugget zone). The processed zone is delimited by a dashed red line in Figure 6a–c. In the nugget zone, the grains were equiaxed and smaller in size. The HAZ was characterized by larger grains, as the cooling rate in this zone was slower. The grains in the HAZ had an orientation according to the rolling direction of the plate.

The parameters used in the AA7_6_1120/180 and AA7_6_900/180 tests resulted in better outcomes. Despite a small defect observed in the lower AA 6082-T651 plate, the micrographs revealed good merging between the two plates, which is expected to provide better homogeneity and distribution of the particles when producing surface composites.

In the experiments where the lower plate was composed of the harder alloy (AA 7075-T651), a "flow arm" phenomenon was observed as this material easily penetrated the upper plate which was made of the softer alloy (AA 6082-T651), as shown in Figure 7a,b. This phenomenon was not observed in experiments where the upper plate was made of the harder alloy (Figure 7c,d). The macrographs presented in Figure 7 highlight that when the AA 6082-T651 plate is placed on the top, a larger defect appears in the lower plate compared to the results obtained with the AA 6082-T651 plate underneath. This occurs because the harder alloy (AA 7075-T651) has more facility in penetrating the softer alloy (AA 6082-T651), resulting in a greater upward flow of material from the lower plate, leading to a larger defect on the lower plate.

(a) AA7_6_1400/71

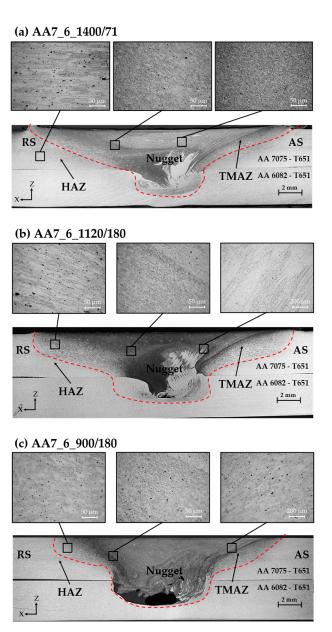**(b) AA7_6_1120/180**

(c) AA7_6_900/180

Figure 6. Micrography of aluminium-based dissimilar alloys composites produced by UFSP with a lower plate of AA 6082-T651 and an upper plate of AA 7075-T651: (**a**) AA7_6_1400/71; (**b**) AA7_6_1120/180; (**c**) AA7_6_900/180.

To indirectly assess the mechanical properties of the produced dissimilar alloys composites, microhardness and eddy currents tests were conducted. Hardness is a property that influences mechanical strength and can be a good indicator to evaluate the mechanical properties of the produced dissimilar alloys composites. Eddy currents tests are non-destructive tests that allow the assessment of electrical conductivity variations and can be used to evaluate microstructural and hardness variations as this is inversely proportional to electrical conductivity, as confirmed by previous studies [1,42,49]. In other words, the nugget zone, which has a finer grain structure and a higher number of grain boundaries, exhibits higher electrical resistance and higher mechanical strength. In contrast, regions with coalesced grains, such as the HAZ, exhibit lower mechanical strength and higher electrical conductivity [49].

The results comparing microhardness and eddy currents measurements presented in Figure 8 corresponded to the tests that yielded the most interesting results for obtaining surface composites. In Figure 8a,b, the microhardness and eddy currents results of the AA7_6_1120/180 and AA7_6_900/180 samples are shown, respectively. In Figure 8a, a

slight decrease ($\approx$20 HV 0.5) in hardness is observed in the stirred zone compared to the base material. This decrease is attributed to the lowering of the strengthening effect induced by the T651 heat treatment due to low-temperature annealing during UFSP. The results of the eddy currents tests are in good agreement with the obtained hardness profiles.
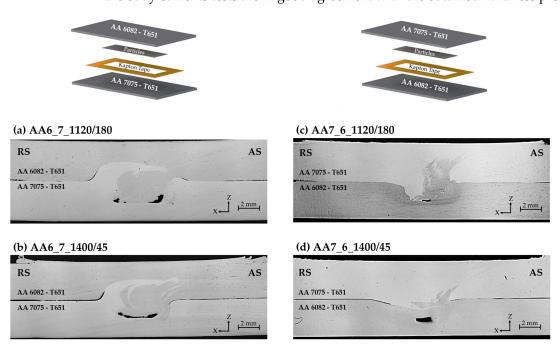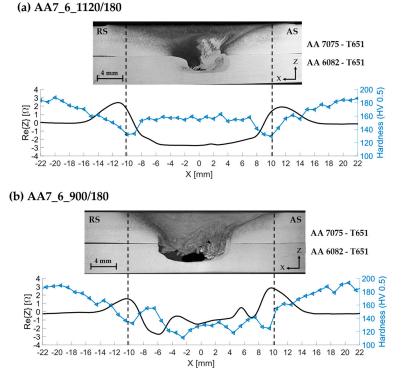

Figure 7. Macrography of aluminium-based dissimilar alloys composites produced by UFSP with a lower plate of AA 7075-T651 and an upper plate of AA 6082-T651: (**a**) AA6_7_1120/180; (**b**) AA6_7_1400/45 and dissimilar alloys composites produced with a lower plate of AA 6082-T651 and an upper plate of AA 7075-T651; (**c**) AA7_6_1120/180; (**d**) AA7_6_1400/45.

Figure 8. Eddy currents and microhardness profiles along the X direction of the plates: (**a**) AA7_6_1120/180 and (**b**) AA7_6_900/180.

In the case of the AA7_6_900/180 sample (Figure 8b), a noticeable decrease in hardness was also observed in the stirred zone compared to the base material. However, this decrease was more significant ($\approx$40 HV 0.5) compared to the AA7_6_1120/180 sample, which may indicate an increased flow of material from the lower plate to the upper plate. This higher material flow is one of the key points of UFSP as it indicates the presence of upward material flow, which promotes better aspiration of particles when producing surface composites.

3.2. Aluminium-Based Dissimilar Alloys Surface Composites Reinforced with SiC Particles

Figure 9 shows the macrographs of aluminium-based dissimilar alloys composites reinforced with SiC particles produced by UFSP. The results presented in Figure 9, where a series of tests were conducted with the incorporation of SiC particles, are consistent with the findings reported in Section 3.1. A comparison was made between the tests carried out with a lower plate of AA 6082-T651 and an upper plate of AA 7075-T651 and tests conducted with a lower plate of AA 7075-T651 and an upper plate of AA 6082-T651.
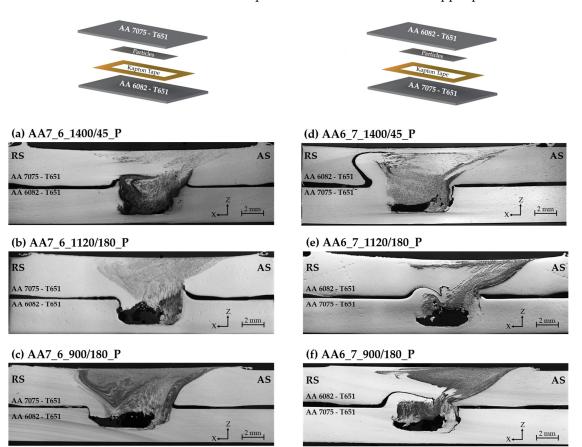

Figure 9. Macrography of aluminium-based dissimilar alloys composites reinforced with SiC particles produced by UFSP with a lower plate of AA 6082-T651 and an upper plate of AA 7075-T651: (**a**) AA7_6_1400/45_P; (**b**) AA7_6_1120/180_P; (**c**) AA7_6_900/180_P and composites produced with a lower plate of AA 7075-T651 and an upper plate of AA 6082-T651; (**d**) AA7_6_1400/45_P; (**e**) AA7_6_1120/180_P; (**f**) AA7_6_900/180_P.

In the tests with AA 7075-T651 as the lower plate (Figure 9d–f), the formation of a "flow arm" was observed penetrating the upper plate as the harder material more easily incorporated into the softer matrix. However, when the order of overlapping was reversed (Figure 9a–c), no "flow arm" formed as the less hard alloy (AA 6082-T651) did not penetrate as easily into the harder alloy (AA 7075-T651).

The formation of the "flow arm" in the tests with the AA 6082-T651 alloy as the upper plate affected the incorporation of particles as the majority of particles were only distributed

on the advancing side and did not reach the upper plate on the retreating side (or the side of the "flow arm"). This can be observed in the macrographs of the samples produced in tests AA7_6_1400/45_P, AA7_6_1120/180_P, and AA7_6_900/180_P (Figure 9d–f).

In the tests with the AA 7075-T651 alloy as the upper plate, the absence of the "flow arm" resulted in a more homogeneous distribution of particles in the upper zone of the nugget, as seen in the macrographs of the samples produced in tests AA7_6_1400/45_P, AA7_6_1120/180_P, and AA7_6_900/180_P (Figure 9a–c).

Overall, better results were obtained when the upper plate was made of AA 7075-T651 with higher hardness than the material of the lower plate (AA 6082-T651). Among the results presented, the sample AA7_6_1400/45_P was discarded due to a macroscopically uneven distribution of SiC particles. In addition, Figure 10 presents micrographs of the AA7_6_1120/180_P and AA7_6_900/180_P samples.
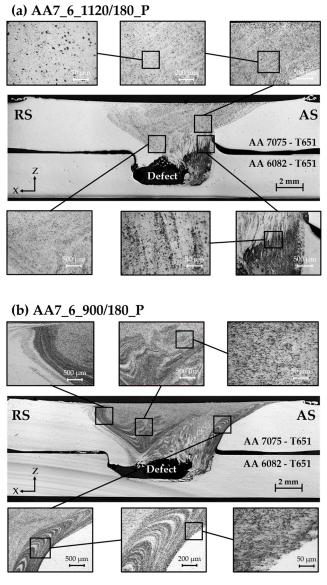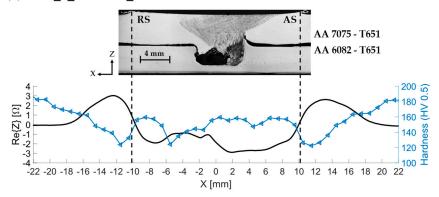
(a) AA7_6_1120/180_P

(b) AA7_6_900/180_P

Figure 10. Micrography of aluminium-based dissimilar alloys composites reinforced with SiC particles produced by UFSP with a lower plate of AA 6082-T651 and an upper plate of AA 7075-T651: (**a**) AA7_6_1120/180_P; (**b**) AA7_6_900/180_P.

Microhardness and eddy currents tests were conducted on the samples that were produced with the same process parameters as shown in Figure 10. Figure 11a,b depict the microhardness and eddy currents testing results of the AA7_6_1120/180_P and

AA7_6_900/180_P samples, respectively. In Figure 11a, a slight reduction of approximately 20 HV 0.5 in hardness is observed in the stirred zone compared to the base material. This decrease is attributed to the weakening effect caused by the low-temperature annealing during UFSP, which reduces the strengthening effect induced by the T651 heat treatment. However, the incorporation of particles did not affect the surface composite hardness in the stirred zone (Figures 8a and 11a). The results of the eddy currents testing agree with the obtained hardness profiles.

(a) AA7_6_1120/180_P

(b) AA7_6_900/180_P

Figure 11. Eddy currents and microhardness profiles along the X direction of the plates reinforced with SiC particles: (**a**) AA7_6_1120/180_P and (**b**) AA7_6_900_180_P.

For the AA7_6_900/180_P sample (Figure 11b), the same hardness was observed in the stirred zone compared to the surface composite shown in Figure 8b. Additionally, the incorporation of particles did not affect the hardness. However, when compared to the base material, a noticeable decrease in the hardness of approximately 40 HV 0.5 was observed in the surface composite AA7_6_900/180_P, which may be attributed to the weakening effect induced by the low-temperature annealing during UFSP, resulting in a decrease in the strengthening effect induced by the T651 heat treatment. The results of the eddy currents testing are also consistent with the obtained hardness profiles.

In summary, the presence of SiC particles did not affect the hardness in the stirred zone, and the UFSP imposed a reduction in the hardness compared to the base material.

Based on the macrographs and micrographs analyses and the microhardness and eddy current tests of the samples produced with SiC particles, it was concluded that the AA7_6_900/180_P sample exhibited a more homogeneous distribution of particles in the nugget zone. Figure 12 shows the processed zone of the AA7_6_900/180_P sample where only a superficial defect is present at the keyhole.
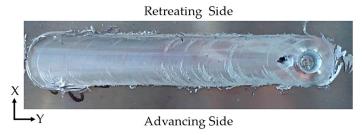
Figure 12. Surface composite AA7_6_900/180_P produced by UFSP with a lower plate of AA 6082-T651 and an upper plate of AA 7075-T651.

Figure 13 depicts EDS mapping images of the surface of sample AA7_6_900/180_P, with the analyses conducted in the nugget zone located on the upper plate, as indicated in Figure 13. The EDS mapping images reveal the presence of Al, Mg, and Si in the sample, indicating the presence of different phases and confirming the incorporation of alloy elements in the surface composite. The mapping images also clearly show that the SiC particles were incorporated into the aluminium matrix material. Additionally, the mapping images highlight the presence of major elements such as Al and Si in sample AA7_6_900/180_P.
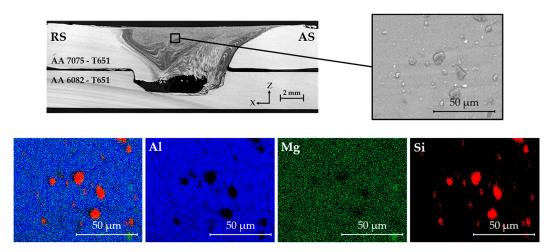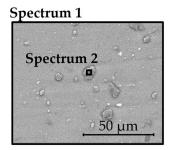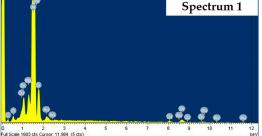

Figure 13. Energy dispersive X-ray spectroscopy (EDS) mapping images of sample AA7_6_900/180_P.

In Figure 14, the analysis of an EDS spectrum image (Spectrum 1) is depicted, which was conducted in the region indicated by a black square. In this analysis, the presence of silicon (Si) was identified, which could be attributed to the proximity of the analyzed region to the SiC particles. This could also be a consequence of the upward flow during the UFSP technique, allowing for the incorporation of the alloy from the lower plate into the upper metal matrix as Si is an element present in AA 6082-T651 (lower plate).
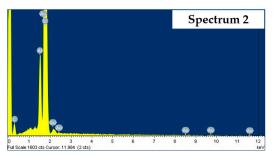

Figure 14. Energy dispersive X-ray spectroscopy (EDS) spectrum images of sample AA7_6_900/180_P.

Further analysis of Spectrum 2 (Figure 14) confirmed the incorporation of SiC particles into the upper metal matrix as the spectrum revealed the presence of silicon (Si) and carbon (C) in significant quantities in the analyzed region. Therefore, these elements can only belong to the silicon carbide (SiC) particles.

Figure 15 displays EDS mapping images that allow for the study of the material "flow arms" on the advancing side. The mapping images revealed that the mixing of the alloys' elements was more intense and homogeneous than what was indicated by the macrographs presented in Figure 9. The mapping images indicate that the alloys from the upper and lower plates were mixed. The "flow arms" of material from the lower plate were also analyzed in Figures 16 and 17. According to the EDS analyses shown in Figures 16 and 17, there was an increase in the atomic weight of certain elements in the upper plate. Specifically, the atomic weights of magnesium (Mg) and zinc (Zn) increased from 1.65% and 0.97% (Figure 16) to 2.58% and 1.98% (Figure 17), respectively. Since these elements are present in both aluminium alloys (AA 6082-T651 and AA 7075-T651), the increase in their atomic weight provides evidence that the lower plate of AA 6082-T651 was mixed with the upper plate of AA 7075-T651. Additionally, Table 5 presents the atomic weights of the elements within the macrography of the stirred zone of sample AA7_6_900/180_P obtained by EDS analysis.
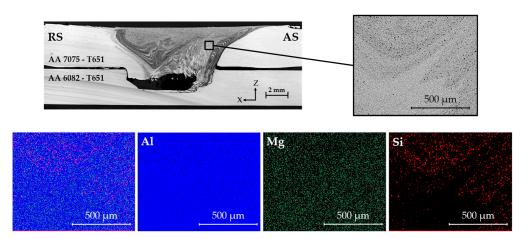

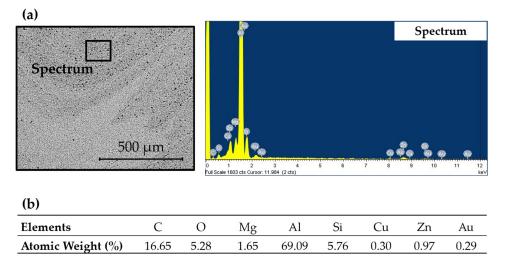**Figure 15.** Energy dispersive X-ray spectroscopy (EDS) mapping images of sample AA7_6_900/180_P in advancing side.

(a)

(b)

Elements	C	O	Mg	Al	Si	Cu	Zn	Au
Atomic Weight (%)	16.65	5.28	1.65	69.09	5.76	0.30	0.97	0.29

Figure 16. Energy dispersive X-ray spectroscopy (EDS) analysis of upper plate in the advancing side of sample AA7_6_900/180_P: (**a**) spectrum image; (**b**) atomic weights of the elements within the sample.

(a)

(b)

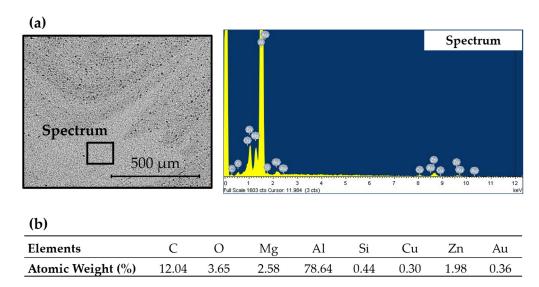| Elements	C	O	Mg	Al	Si	Cu	Zn	Au
Atomic Weight (%)	12.04	3.65	2.58	78.64	0.44	0.30	1.98	0.36

Figure 17. Energy dispersive X-ray spectroscopy (EDS) analysis of the "flow arms" in the advancing side of sample AA7_6_900/180_P: (**a**) spectrum image; (**b**) atomic weights of the elements within the sample.

Table 5. Atomic weights of the elements within the sample AA7_6_900/180_P obtained by EDS analysis.

Elements	Al	Mg	Zn	Cu	O	Si	C	Au
Atomic Weight (%)	69.64	1.55	1.18	0.33	4.31	6.29	16.42	0.28

4. Conclusions

Through the observation of AA7_6_1400/45_P and AA6_7_1400/45_P tests, it was concluded that the parameters that resulted in good bonding between the plates without particles (with minimal internal defects) did not yield favourable results when the particles were incorporated. Thus, not all parameter combinations that result in good bonding between the plates correspond to parameters that achieve effective particle incorporation.

Despite high rotational speeds (typically between 1000 and 2000 rev/min) and low traverse speeds (between 100 and 20 mm/min) being considered optimal for overlapped FSW joints, these parameters did not result in the best particle distribution. The AA7_6_1120/180_P and AA7_6_900/180_P tests yielded better results, with AA7_6_900/180_P being the most successful one. In the AA7_6_900/180_P test, the rotational speed was 900 rev/min, and the traverse speed was 180 mm/min. The upper plate was made of AA 7075-T651, and the lower plate was made of AA 6082-T651.

The production of aluminium-based dissimilar alloys surface composites reinforced with SiC particles led to the following conclusions.

- A reduction of approximately 20 HV 0.5 in hardness was observed in the stirred zone when compared to the base material. This reduction can be attributed to the weakening effect caused by low-temperature annealing during UFSP, which reduces the strengthening effect induced by the T651 heat treatment.
- The presence of particles did not influence the surface composites' hardness in the stirred zone.
- The findings from the eddy currents tests are in good agreement with the hardness profiles obtained.
- The lower plate was not found to be a merely sacrificial plate. Despite significant internal defects observed after processing, SEM analyses revealed evidence of merging of the lower alloy into the upper zone.

- The production of bimetallic composites through UFSP may offer advantages over composites produced from a monometallic matrix as there were significant changes in the chemical composition of the upper plate.
- The results of the eddy currents testing and microhardness measurements were consistent with the SEM/EDS analyses.

References

1. Ferreira, P.M.; Machado, M.A.; Carvalho, M.S.; Vidal, C. Granting Sensorial Properties to Metal Parts through Friction Stir Processing. *Meas. J. Int. Meas. Confed.* **2023**, *207*, 112405. [CrossRef]
2. Sunil, B.R.; Reddy, G.P.K.; Patle, H.; Dumpala, R. Magnesium Based Surface Metal Matrix Composites by Friction Stir Processing. *J. Magnes. Alloy.* **2016**, *4*, 52–61. [CrossRef]
3. Sharma, V.; Prakash, U.; Kumar, B.V.M. Surface Composites by Friction Stir Processing: A Review. *J. Mater. Process. Technol.* **2015**, *224*, 117–134. [CrossRef]
4. Khan, M.A.; Butola, R.; Gupta, N. A Review of Nanoparticle Reinforced Surface Composites Processed by Friction Stir Processing. *J. Adhes. Sci. Technol.* **2023**, *37*, 565–601. [CrossRef]
5. Omotehinse, I.S.; Abioye, T.E.; Anasyida, A.S.; Omiyale, B.O. Review of Parametric Strategies for Enhancing the Mechanical and Wear Properties of Friction Stir Processed Aluminium Alloys Composites. *Trans. Indian Inst. Met.* **2023**, *76*. [CrossRef]
6. Bharti, S.; Ghetiya, N.D.; Patel, K.M. A Review on Manufacturing the Surface Composites by Friction Stir Processing. *Mater. Manuf. Process.* **2021**, *36*, 135–170. [CrossRef]
7. Das, S.S.; Raja, A.R.; Nautiyal, H.; Gautam, R.K.S.; Jha, P.; Sharma, J.; Singh, S. A Review on Aluminum Matrix Composites Synthesized by FSP. *Macromol. Symp.* **2023**, *407*, 2200119. [CrossRef]
8. Vasava, A.; Singh, D. Influence of Various Tool Shoulder Design on Hybrid Surface Composite of AA7075-T651/SiC/Graphene through Friction Stir Processing. *Can. Metall. Q* **2023**, *62*, 1–19. [CrossRef]
9. Liao, Z.; Abdelhafeez, A.; Li, H.; Yang, Y.; Diaz, O.G.; Axinte, D. State-of-the-Art of Surface Integrity in Machining of Metal Matrix Composites. *Int. J. Mach. Tools Manuf.* **2019**, *143*, 63–91. [CrossRef]
10. Singh, L.; Singh, B.; Saxena, K.K. Manufacturing Techniques for Metal Matrix Composites (MMC): An Overview. *Adv. Mater. Process. Technol.* **2020**, *6*, 441–457. [CrossRef]
11. Kumar Sharma, A.; Bhandari, R.; Aherwar, A.; Rimašauskienė, R.; Pinca-Bretotean, C. A Study of Advancement in Application Opportunities of Aluminum Metal Matrix Composites. *Mater. Today Proc.* **2020**, *26*, 2419–2424. [CrossRef]
12. Ferreira, P.M.; Machado, M.A.; Carvalho, M.S.; Vidal, C. Embedded Sensors for Structural Health Monitoring: Methodologies and Applications Review. *Sensors* **2022**, *22*, 8320. [CrossRef]
13. Singh, R.K.; Gilbert, D.R.; Fitz-Gerald, J.; Lee, D.G. Surface Composites: Novel Method to Fabricate Adherent Interfaces. *Surf. Eng.* **1997**, *13*, 389–392. [CrossRef]
14. Riabkina-Fishman, M.; Rabkin, E.; Levin, P.; Frage, N.; Dariel, M.; Weisheit, A.; Galun, R.; Mordike, B. Laser Produced Functionally Graded Tungsten Carbide Coatings on M2 High-Speed Tool Steel. *Mater. Sci. Eng. A* **2001**, *302*, 106–114. [CrossRef]
15. Ayers, J.D.; Tucker, T.R. Particulate-TiC-Hardened Steel Surfaces by Laser Melt Injection. *Thin Solid Films* **1980**, *73*, 201–207. [CrossRef]

16. Farayibi, P.K.; Folkes, J.A.; Clare, A.T. Laser Deposition of Ti-6Al-4V Wire with WC Powder for Functionally Graded Components. *Mater. Manuf. Process.* **2013**, *28*, 514–518. [CrossRef]

17. Wang, X.H.; Zhang, M.; Du, B.S. Fabrication of Multiple Ceramic Particle Reinforced Iron Matrix Coating by Laser Cladding. *Mater. Manuf. Process.* **2013**, *28*, 509–513. [CrossRef]

18. Mehdi, H.; Mishra, R.S. Consequence of Reinforced SiC Particles on Microstructural and Mechanical Properties of AA6061 Surface Composites by Multi-Pass FSP. *J. Adhes. Sci. Technol.* **2022**, *36*, 1279–1298. [CrossRef]

19. Srivastava, M.; Rathee, S.; Siddiquee, A.N.; Maheshwari, S. Investigation on the Effects of Silicon Carbide and Cooling Medium during Multi-Pass FSP of Al-Mg/ SiC Surface Composites. *Silicon* **2019**, *11*, 2149–2157. [CrossRef]

20. Patel, K.; Ghetiya, N.D.; Bharti, S. Effect of Single and Double Pass Friction Stir Processing on Microhardness and Wear Properties of AA5083/Al2O3 Surface Composites. *Mater. Today Proc.* **2022**, *57*, 38–43. [CrossRef]

21. Dilip, J.J.S.; Babu, S.; Rajan, S.V.; Rafi, K.H.; Ram, G.D.J.; Stucker, B.E. Use of Friction Surfacing for Additive Manufacturing. *Mater. Manuf. Process.* **2013**, *28*, 189–194. [CrossRef]

22. Li, B.; Shen, Y.; Lei, L.; Hu, W. Fabrication and Evaluation of Ti₃Alₚ/Ti–6Al–4V Surface Layer via Additive Friction-Stir Processing. *Mater. Manuf. Process.* **2014**, *29*, 412–417. [CrossRef]

23. Li, B.; Shen, Y.; Hu, W. Friction-Stir Nitriding of Titanium Alloy Surface Layer. *Mater. Manuf. Process.* **2014**, *29*, 493–497. [CrossRef]

24. Akinlabi, E.T.; Andrews, A.; Akinlabi, S.A. Effects of Processing Parameters on Corrosion Properties of Dissimilar Friction Stir Welds of Aluminium and Copper. *Trans. Nonferrous Met. Soc. China* **2014**, *24*, 1323–1330. [CrossRef]

25. Zheng, Q.; Feng, X.; Shen, Y.; Huang, G.; Zhao, P. Effect of Plunge Depth on Microstructure and Mechanical Properties of FSW Lap Joint between Aluminum Alloy and Nickel-Base Alloy. *J. Alloys Compd.* **2017**, *695*, 952–961. [CrossRef]

26. Beygi, R.; Mehrizi, M.Z.; Verdera, D.; Loureiro, A. Influence of Tool Geometry on Material Flow and Mechanical Properties of Friction Stir Welded Al-Cu Bimetals. *J. Mater. Process. Technol.* **2018**, *255*, 739–748. [CrossRef]

27. Vasava, A.; Singh, D. Effect of Different Volume Ratios of SiC and TiO₂ Reinforcement Particles on Mono and Hybrid Surface Composites of AA7075-T651 through Friction Stir Processing. *J. Adhes. Sci. Technol.* **2023**, *4*, 1–20. [CrossRef]

28. Khan, N.Z.; Siddiquee, A.N.; Khan, Z.A.; Mukhopadhyay, A.K. Mechanical and Microstructural Behavior of Friction Stir Welded Similar and Dissimilar Sheets of AA2219 and AA7475 Aluminium Alloys. *J. Alloys Compd.* **2017**, *695*, 2902–2908. [CrossRef]

29. Leitão, C.; Louro, R.; Rodrigues, D.M. Analysis of High Temperature Plastic Behaviour and Its Relation with Weldability in Friction Stir Welding for Aluminium Alloys AA5083-H111 and AA6082-T6. *Mater. Des.* **2012**, *37*, 402–409. [CrossRef]

30. Gungor, B.; Kaluc, E.; Taban, E.; Sik, A. Mechanical, Fatigue and Microstructural Properties of Friction Stir Welded 5083-H111 and 6082-T651 Aluminum Alloys. *Mater. Des.* **2014**, *56*, 84–90. [CrossRef]

31. Amancio-Filho, S.T.; Sheikhi, S.; dos Santos, J.F.; Bolfarini, C. Preliminary Study on the Microstructure and Mechanical Properties of Dissimilar Friction Stir Welds in Aircraft Aluminium Alloys 2024-T351 and 6056-T4. *J. Mater. Process. Technol.* **2008**, *206*, 132–142. [CrossRef]

32. Moradi, M.M.; Jamshidi Aval, H.; Jamaati, R.; Amirkhanlou, S.; Ji, S. Microstructure and Texture Evolution of Friction Stir Welded Dissimilar Aluminum Alloys: AA2024 and AA6061. *J. Manuf. Process.* **2018**, *32*, 1–10. [CrossRef]

33. Farhang, M.; Mohammadreza Farahani, M.N.; Sam-Daliri, O. Experimental Correlation Between Microstructure, Residual Stresses and Mechanical Properties of Friction Stir Welded 2024-T6 Aluminum Alloys. *Int. J. Adv. Des. Manuf. Technol.* **2022**, *15*, 1–9. [CrossRef]

34. Çavuşoğlu, N. Effect of Friction Welding Parameters on the Mechanical and Microstructural Properties of Dissimilar IN713C-AISI 4140 Joints. *J. Mater. Eng. Perform.* **2022**, *31*, 4035–4048. [CrossRef]

35. Farhang, M.; Sam-Daliri, O.; Farahani, M.; Vatani, A. Effect of Friction Stir Welding Parameters on the Residual Stress Distribution of Al-2024-T6 Alloy. *J. Mech. Eng. Sci.* **2021**, *15*, 7684–7694. [CrossRef]

36. Guo, J.F.; Chen, H.C.; Sun, C.N.; Bi, G.; Sun, Z.; Wei, J. Friction Stir Welding of Dissimilar Materials between AA6061 and AA7075 Al Alloys Effects of Process Parameters. *Mater. Des.* **2014**, *56*, 185–192. [CrossRef]

37. Sahu, P.K.; Pal, S.; Pal, S.K.; Jain, R. Influence of Plate Position, Tool Offset and Tool Rotational Speed on Mechanical Properties and Microstructures of Dissimilar Al/Cu Friction Stir Welding Joints. *J. Mater. Process. Technol.* **2016**, *235*, 55–67. [CrossRef]

38. Cavaliere, P.; De Santis, A.; Panella, F.; Squillace, A. Effect of Welding Parameters on Mechanical and Microstructural Properties of Dissimilar AA6082–AA2024 Joints Produced by Friction Stir Welding. *Mater. Des.* **2009**, *30*, 609–616. [CrossRef]

39. Dinaharan, I.; Kalaiselvan, K.; Vijay, S.J.; Raja, P. Effect of Material Location and Tool Rotational Speed on Microstructure and Tensile Strength of Dissimilar Friction Stir Welded Aluminum Alloys. *Arch. Civ. Mech. Eng.* **2012**, *12*, 446–454. [CrossRef]

40. Prasad, B.L.; Neelaiah, G.; Krishna, M.G.; Ramana, S.V.V.; Prakash, K.S.; Sarika, G.; Reddy, G.P.K.; Dumpala, R.; Sunil, B.R. Joining of AZ91 Mg Alloy and Al6063 Alloy Sheets by Friction Stir Welding. *J. Magnes. Alloy.* **2018**, *6*, 71–76. [CrossRef]

41. Fu, B.; Qin, G.; Li, F.; Meng, X.; Zhang, J.; Wu, C. Friction Stir Welding Process of Dissimilar Metals of 6061-T6 Aluminum Alloy to AZ31B Magnesium Alloy. *J. Mater. Process. Technol.* **2015**, *218*, 38–47. [CrossRef]

42. Inácio, P.L.; Nogueira, F.; Ferreira, F.B.; Vidal, C.; Schell, N.; Tero, T.; Vilaça, P.; Oliveira, J.P.; Santos, T.G. Functionalized Material Production via Multi-Stack Upward Friction Stir Processing (UFSP). *Mater. Manuf. Process.* **2022**, *37*, 11–24. [CrossRef]

43. Vidal, C.; Alves, P.; Alves, M.M.; Carmezim, M.J.; Fernandes, M.H.; Grenho, L.; Inácio, P.L.; Ferreira, F.B.; Santos, T.G.; Santos, C. Fabrication of a Biodegradable and Cytocompatible Magnesium/Nanohydroxyapatite/Fluorapatite Composite by Upward Friction Stir Processing for Biomedical Applications. *J. Mech. Behav. Biomed. Mater.* **2022**, *129*, 105137. [CrossRef]

44. Milosan, I.; Bedő, T.; Gabor, C.; Munteanu, D.; Pop, M.A.; Catana, D.; Cosnita, M.; Varga, B. Characterization of Aluminum Alloy–Silicon Carbide Functionally Graded Materials Developed by Centrifugal Casting Process. *Appl. Sci.* **2021**, *11*, 1625. [CrossRef]

45. Tamadon, A.; Pons, D.; Sued, K.; Clucas, D. Development of Metallographic Etchants for the Microstructure Evolution of A6082-T6 BFSW Welds. *Metals* **2017**, *7*, 423. [CrossRef]

46. Zamani, M.H.; Divandari, M.; Tamizifar, M. On the Characteristics of Friction Stir Welding Lap Joint of Magnesium and Aluminum. *Iran. J. Mater. Sci. Eng.* **2018**, *15*, 64–77. [CrossRef]

47. Gao, Y.; Morisada, Y.; Fujii, H.; Liao, J. Dissimilar Friction Stir Lap Welding of Magnesium to Aluminum Using Plasma Electrolytic Oxidation Interlayer. *Mater. Sci. Eng. A* **2018**, *711*, 109–118. [CrossRef]

48. Grimm, A.; Schulze, S.; Silva, A.; Göbel, G.; Standfuss, J.; Brenner, B.; Beyer, E.; Füssel, U. Friction Stir Welding of Light Metals for Industrial Applications. *Mater. Today Proc.* **2015**, *2*, S169–S178. [CrossRef]

49. Sorger, G.L.; Oliveira, J.P.; Inácio, P.L.; Enzinger, N.; Vilaça, P.; Miranda, R.M.; Santos, T.G. Non-Destructive Microstructural Analysis by Electrical Conductivity: Comparison with Hardness Measurements in Different Materials. *J. Mater. Sci. Technol.* **2019**, *35*, 360–368. [CrossRef]